Computers in Biology and Medicine 44 (2014) 144–157

Contents lists available at ScienceDirect

Computers in Biology and Medicine

journal homepage: www.elsevier.com/locate/cbm

Detection of pigment network in dermoscopy images using supervised machine learning and structural analysis

Jose Luis García Arroyo *, Begoña García Zapirain

Deustotech-LIFE Unit (eVIDA). University of Deusto. Avda. Universidades, 24. 48007 Bilbao, Spain

ARTICLE INFO

Article history:
Received 24 June 2013
Accepted 3 November 2013

Keywords:
Melanoma
Machine learning
Pigment network
Structural analysis
Reticular pattern

ABSTRACT

By means of this study, a detection algorithm for the "pigment network" in dermoscopic images is presented, one of the most relevant indicators in the diagnosis of melanoma. The design of the algorithm consists of two blocks. In the first one, a machine learning process is carried out, allowing the generation of a set of rules which, when applied over the image, permit the construction of a mask with the pixels candidates to be part of the pigment network. In the second block, an analysis of the structures over this mask is carried out, searching for those corresponding to the pigment network and making the diagnosis, whether it has pigment network or not, and also generating the mask corresponding to this pattern, if any. The method was tested against a database of 220 images, obtaining 86% sensitivity and 81.67% specificity, which proves the reliability of the algorithm.

1. Introduction

Melanoma is a type of skin cancer that represents approximately 1.6% of the total number of cancer cases worldwide [1]. In the fight against this type of cancer, early detection is a key factor: if detected early, before the tumor has penetrated the skin (non-invasive melanoma or melanoma in situ), the survival rate is 98%, falling to 15% in advanced cases (invasive melanoma), when the tumor has spread (metastasized) [2].

In the detection of melanoma, the most commonly used technique is dermoscopy, which consists of a skin examination through an optical system attached to a light source, which allows its magnification, thus enabling the visualization in depth of structures, forms and colors that are not accessible to a simple visual inspection [3]. It also allows reproducibility in the diagnosis, as well as the use of digital image processing techniques. There are also new encouraging techniques other than dermoscopy [4–8]; notwithstanding, given its facility for image acquisition, its good results and its high degree of utilization among medical experts, its use for a long period of time is ensured; in fact, dermoscopy has been recognized as the "gold standard" in the screening phase [8].

In order to carry out the diagnosis, the most frequently used method is the "Two-Step Procedure" in which, as its name suggests, the diagnosis is carried out in two steps. In the first step the dermatologist must discern whether it is a melanocytic lesion or not, on the basis of a series of criteria. If not, the lesion is not a melanoma. In affirmative case, the second step is reached, in which a diagnostic method is used to calculate the degree of malignancy, on the basis of which it is decided whether a biopsy should be performed [3]. The most commonly used methods are "Pattern Analysis" [9] or the so-called medical algorithms, such as the "ABCD Rule" [10], the "Menzies Method" [11] and the "7-point-Checklist" [12]. All of them aim to quantitatively detect and characterize a series of indicators observed by the doctors and to undertake the diagnosis based on pre-established ranges of values. Some of the most relevant indicators are the dermoscopic patterns or structures, such as pigment network, streaks, globules, dots, blue-white veil, blotches or regression structures. It should be noted, however, that the objectification is particularly difficult and, in many cases, is highly biased by the subjectivity of the dermatologists.

One of the most relevant dermoscopic structures is the pigment network, also called reticular pattern, which presence is an indicator of the existence of melanin deep inside the layers of the skin. It is of great importance, since it is one of the key criteria for the determination of a melanocytic lesion in the first step of the so-called "Two-Step Procedure", being moreover an indicator present in all the medical methods for the diagnosis of melanoma. The name is derived from the form of this structure, which resembles a net, darker in color than the "holes" it forms, corresponding to the lesion's background. Two examples representing this structure can be seen in Fig. 1. There are two types of pigment network: the typical one, with a light-to dark-brown net with small, uniformly spaced holes and thin lines distributed more or less regularly, and the atypical one, which is a black, brown or gray net with irregular holes and thick lines, frequently being an indicator of melanoma [3].

* Corresponding author. Deustotech-Life Unit, Faculty of Engineering, University of Deusto, Av. de las Universidades, 24, 48007 Bilbao, Spain. Tel.: +34 944139000.
E-mail addresses: jlgarcia@deusto.es (J.L. García Arroyo), mbgarciazapi@deusto.es (B. García Zapirain).

0010-4825
http://dx.doi.org/10.1016/j.compbiomed.2013.11.002

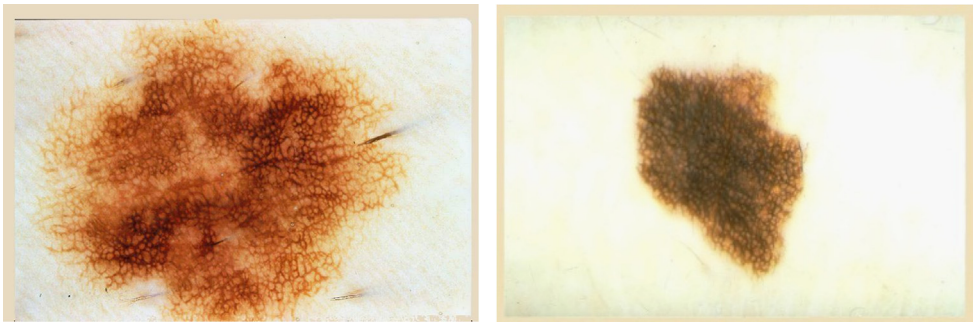

Fig. 1. Two examples of pigment network.

The aim of the presented work is to carry out the automated detection of the pigment network, proposing in this paper an innovative algorithm based on supervised machine learning techniques and structural shape detection.

The paper has been structured as follows: in Section 2 an analysis of the most relevant works of the state of the art concerning the detection of the pigment network is conducted, together with a description of the contribution made. In Section 3 the design of the proposed algorithm is explained in detail, in Section 4 the results of the algorithm are shown, undertaking a discussion on them in Section 5 and, finally, in Section 6 the conclusions and future research lines are presented.

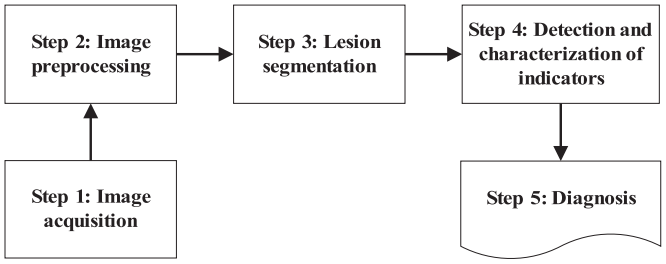

Fig. 2. Stages of the life cycle of an automated system for the detection of melanoma.

2. State of the art

2.1. Overview of automatic detection of pigment network

For the automated detection of melanoma over dermoscopic images, various CAD systems have been presented recently, this being a current object of research [13].

As can be seen in Fig. 2, the life cycle of a CAD of this kind consists of the following stages: (1) image acquisition; (2) image preprocessing, the main task of which is the detection and removal of artifacts, especially hairs; (3) skin lesion segmentation; (4) detection and characterization of indicators; (5) diagnosis.

In the design of stages 4 and 5 there are two different approaches. A first approach, used for example in the classic work [14] or in the most recent ones [15,16], uses supervised machine learning, consisting in the first place on the extraction of different types of features from the dermoscopic image and subsequently carrying out the diagnosis by means of the classifier generated. A second approach, used for example in [17,18] and in most of the commercial systems described in [19], consists in reproducing as faithfully as possible a medical algorithm, calculating the values of the indicators and obtaining the degree of malignancy, using the corresponding formula. This approach is the most common one, since the doctor, who takes the final decision, prefers to rely on a well-known algorithm. In all of them, some of the most relevant indicators are the dermoscopic patterns or structures. Some relevant works related to its detection and characterization are considered in pigment network (these will be described later), streaks [20–22], globules and dots [23–25], blue-white veil [26–28]), vascular [29], blotches [30–32], hypopigmentation [33], regression structures [27,34] and parallel pattern [35].

The automated detection of the pigment network is a challenging problem, since it is a complex one for different reasons. Sometimes, there is a low contrast between the net and the background; moreover, the size of the net holes may comprise considerably different sizes in different images, and even in the same image there often exists big irregularities in shape and size.

2.2. Previous works in pigment network detection

The most relevant studies published to date concerning the detection of pigment network are described thereupon.

In [36], Fleming et al. carry out the detection of the pigment network using the Steger curvilinear lines detection algorithm for the extraction of the net and the snakes Lobregt–Viergever model to segment the holes. It is an interesting work, in which 69 images were used (16 common nevi, 22 dysplastic nevi and 31 melanomas), and with ANOVA interesting statistical results were found, related to the correlations of those type of images with net lines widths and hole areas. Nevertheless, no outcome concerning the behavior of the system in the differentiation between “Pigment network” and “No pigment network” was reported.

In [37], Anantha et al. use the Dullrazor software [38] for hair detecting, removing and repairing and two different methods for pigment network detection. These are two texture analysis algorithms, the first one using Law's energy masks and the second one Neighborhood Gray-Level Dependence Matrix (NGLDM), and subsequently conducting a comparison between them, obtaining better results with the first one. The system was tested over a total number of 155 images, obtaining 80% accuracy. This is an interesting work, having nonetheless a weakness due to the use of the Dullrazor software, firstly due to the dependence of the method on this preprocessing software and secondly due to the negative consequences of the errors made by this software, which implies the failure of the reticular detection algorithm; in fact, most of the errors reported by the authors have the origin in this cause.

In [39], Grana et al. undertake the detection of the pigment network using Gaussian derivative kernels for the detection of the net edges and by means of Fisher linear discriminant analysis obtain the optimal thresholds in the delineation of the structure.

Additionally, a distinction between "no network", "partial network" and "complete network" is made in the images to differentiate whether it is local or global. The algorithm was tested over 60 images, obtaining some interesting partial results related to some thresholds. However, the conducted tests are not focused on the task of discerning between"Pigment network" and "No pigment network", presenting no result in this regard.

In [29], Betta et al. conduct the detection of the atypical pigment network by combining two techniques, a structural one, in which morphological methods are used, and another spectral one, in which FFT, high-pass filters, inverse FFT and finally thresholding techniques are used. The algorithm was tested over 30 images, with no reported results. In [40], Di Leo et al. from the same research group improve on the previous study, defining 9 chromatic and 4 spatial features related to the obtained structures, and using decision tree classifiers, in the categories "Absent", "Typical" and "Atypical", generated by the C4.5 algorithm. The process was conducted over 173 images with more than 85% sensitivity and specificity (no exact values are set). This is a very interesting work, nevertheless they do not report any result about the differentiation between "Pigment network" (that would correspond to "Absent") and "No pigment network" (that would correspond to "Typical" and "Atypical"). Additionally, the management of distortive artifacts (hairs, etc.) is not reported.

In [41], Shrestha et al. use 10 different texture measures for the analysis of the atypical pigment network (APN), calculating the values and using different classifiers. The method was tested with 106 images, obtaining 95.4% accuracy in the detection of APN. This is an interesting method in the detection of APN, however it does not deal with the problem of discerning between "Pigment network" and "No pigment network".

In [42], Sadeghi et al. carry out the detection of the pigment network using the Laplacian of Gaussian (LoG) filter in the first place in order to properly capture the "clear-dark-clear" changes. Then, over the binary image generated, cyclical subgraphs are searched using the ILCA (Iterative Loop Counting Algorithm) algorithm. 500 images were tested with 94.3% accuracy. In [43], Sadeghi et al., from the same research group, improve the algorithm and extend the previous study presenting a new method for classification between "Absent", "Typical" and "Atypical'. To do so, an algorithm based on the previous work is proposed, which detects the net structure and extracts structural, geometric, chromatic and texture features, generating the classification model with the LogitBoost algorithm. 82.3% accuracy is obtained over 436 images. In the experiments concerning both the "Absent" and "Present" categories, 93.3% accuracy is obtained. This is an important work, which presents excellent results.

In [44], Skrovseth et al. use different texture measures for the detection of the pigment network. No information is presented either on the image database used or the results obtained.

In [25], Gola et al. undertake the detection of pigment network by combining morphological techniques with an edge detection algorithm. The method was tested over 40 images, reaching 100% sensitivity and 92.86% specificity. This is an interesting work, however the database used has very few images and it is not possible to evaluate the robustness of the method adequately.

In [45], Wighton et al. present an algorithm for the detection of hair and pigment network based on supervised machine learning, using color and spectral features, followed by LDA for the reduction of dimensionality and Bayesian methods for the model generation. The test was carried out over a total amount of 734 images, without reported results. This is an interesting work, especially with regard to the hair detection.

In [46], Barata et al. undertake the detection of pigment network using a bank of directional filters and morphological operations, followed by a feature extraction and an AdaBoost algorithm for the classification, obtaining a sensitivity of 91.1% and a specificity of 82.1% over a database of 200 images. This is an interesting work, which presents excellent results, also testing the reliability of the algorithm against the masks segmented by experts.

2.3. Contribution of the presented work

Despite the importance of the previously discussed methods there are some questions that must be addressed.

In the first place, in some works, even though interesting algorithms were presented, no result was reported or, if so, they were related to another issues that are not the differentiation between "Pigment network" and "No pigment network". Secondly, most of them assume previous preprocessing and segmentation; therefore they are not able to be used against original images, with hairs or other distortive artifacts (rules, bubbles, etc.), which implies a dependence that restricts the scope of the methods and, in addition, an error in any of the steps could result in a mistake in the detection of the reticular structure. In the third place, the works do not take into account the issues concerning the resolution and magnification of dermoscopic images; the values corresponding to the used datasets are described and the algorithms are developed; however, no parameterization is conducted, a specification of the algorithm extension points facing to scale to another resolution and magnification values is missing.

The presented method improves the state of the art in the previous topics. It is also considered as a contribution, which is in itself a reason that justifies the creation of a new approach and in our opinion covers a gap in the state of the art, the design of a new algorithm that meets simultaneously the following conditions: (1) to have an innovative and good design, simple and complete; (2) to be based on highly regarded technologies in image processing and machine learning fields; (3) to be easily scalable, that is to say, the improvements and extensions are easy to undertake; (4) to gain a high degree of reliability.

3. Proposed design

In this section the proposed design of this system for the detection of pigment network is presented. It is an innovative algorithm, based on supervised machine learning and structural analysis techniques. Hereafter, it is going to be described in detail. In the first place, the high level design of the system is going to be explained and, secondly, the low level design will be shown.

3.1. High level design

The high-level view of the algorithm is presented in Fig. 3. As can be seen, there are two main blocks in the pigment network detection process. In the first place, a machine learning process is carried out, enabling the generation of a set of rules which, when applied to the image, allows obtaining a mask with the pixels candidates that may be part of the pigment network. Secondly, this mask is processed searching for the structures of the pattern, in order to obtain the diagnosis, that is to say, whether it has pigment network or not, and in addition to generating the mask corresponding to such structure, if any.

Either way, it is noteworthy way that the main aim is to accomplish the diagnosis, whether it has pigment network or not, the precise obtaining of the corresponding mask being a secondary issue.

The detection of the reticular pattern would be located within stage 4 of the life cycle of an automated system for the detection of melanoma, which scheme is shown in Fig. 2, the presence of the

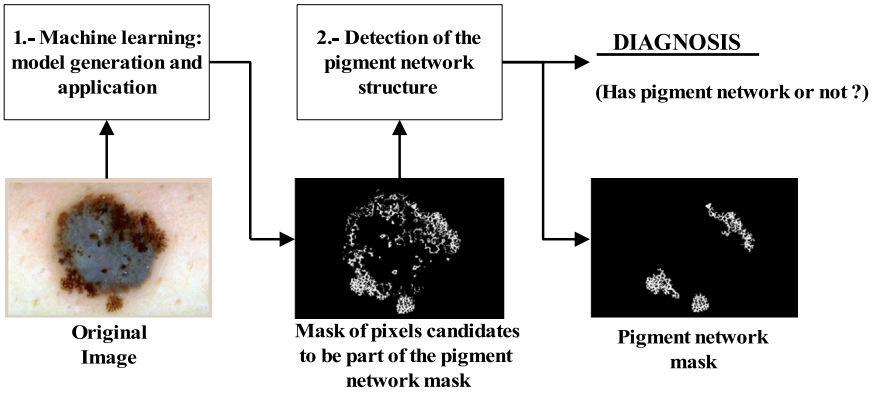

Fig. 3. High level view of the system.

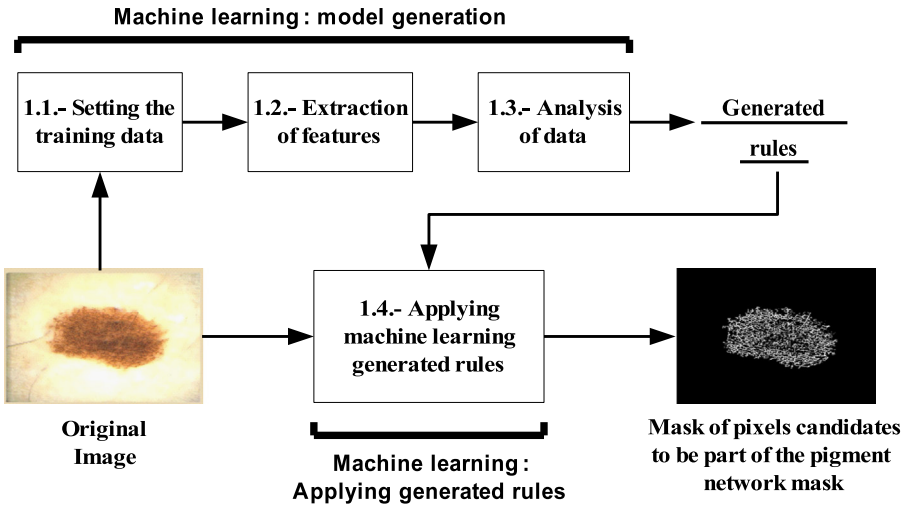

Fig. 4. Design of Block 1. – Machine learning: model generation and application.

pigment network being an indicator to be used in any of the medical methods for melanoma diagnosis, as in the "D" of the "ABCD rule", for example. In any case, the algorithm was designed in such a way that it can be executed directly over the original image, after stage 1. Therefore, the design of our method admits the possibility that there may be hairs or another distortive artifacts in the image, which are commonly eliminated in the preprocessing stage (in stage 2), or the lesion may not have been segmented (in stage 3).

Furthermore, even though the images used in the development and testing of the algorithm have certain resolution and magnification values, this proposed algorithm has been designed with the aim of being able to be reproduced in images with other values. This does not mean that the method is robust with respect to any resolution and magnification, which would imply that the algorithm itself could be used in images with any resolution and magnification. This means that in the design of the algorithm a parameterization has been done, identifying the threshold values which would have to be calculated in the adaptation of the algorithm to images with other values of resolution and magnification.

3.2. Low level design

The low level design of the algorithm will be presented thereupon, explaining in detail each of the relevant blocks and sub-blocks.

3.2.1. Block 1: Machine learning: model generation and application

In this block, a supervised machine learning process is conducted, with the aim of obtaining the pixels candidates to be part of the pigment network, which is performed in two stages. Firstly, the rules to be satisfied by such pixels are obtained, as a statistical classifier. Secondly, the generated rules are applied over the image, obtaining as a result the mask with the pixels candidates.

In a typical case, the input parameter of the algorithm will be the already preprocessed image, with the lesion segmentation already obtained. In any case, as mentioned before, the algorithm admits the possibility of treating the image directly without preprocessing it.

The design of this block can be observed in Fig. 4. As can be seen, the process consists of 4 stages. In the first place, the setting of training data is carried out. Secondly, the extraction of the features is performed in order to feed the machine learning process. Obviously, the chosen features are those that have been considered to be the most suitable ones for the characterization of the pixels that are part of a pigment network, as will be explained below. Thirdly, the analysis of the data is conducted, obtaining as a result the construction of a classification model, implementation of the generated rules. Finally, in the fourth place, the generated rules are applied to the image, obtaining the mask corresponding to the set of pixels candidates to be part of the pigment network.

With respect to the parameterization of the method, according to the resolution and magnification values, two threshold values were defined in this block: σ_{max} (and its corresponding m_{max}) in

the extraction of the spectral texture features, and n_{max}, in the extraction of the statistical texture features, which are to be discussed later.

Sub-block 1.1. – *Setting the training data*: The aim of this machine learning process is to obtain the rules to be fulfilled by the pixels candidate to be part of a reticular structure. On the basis of such objective, a total number of 40 images were selected, 25 of them with the reticular pattern. Over these images, with the help of two expert dermatologists, mentioned below in the Results section, there were selected different samples of reticular and non-reticular pixels, up to a total of 400 for each case, thus obtaining a total number of 800 different samples.

With the objective of being able to analyze the not preprocessed images, there were included among the samples, as non-reticular pixels, various corresponding to artifacts commonly presented in the original images (hairs, rules, etc.) and pixels corresponding to skin.

Sub-block 1.2. – *Extraction of features*: As can be seen in Fig. 5, three types of features were extracted for the generation of the model: from the original image the extraction of color features was conducted, with the aim of characterizing the color of the reticular pixels; subsequently, from the image transformed to the gray scale, the extraction of spectral and statistical texture features was conducted, with the aim of characterizing the reticular texture.

The choice of the features is obviously derived from the nature of the reticular structures. All of them are widely known in image processing and they have been used over the past few years in many investigations of this type with good results. The motivation for each one of them will be discussed in the following sections.

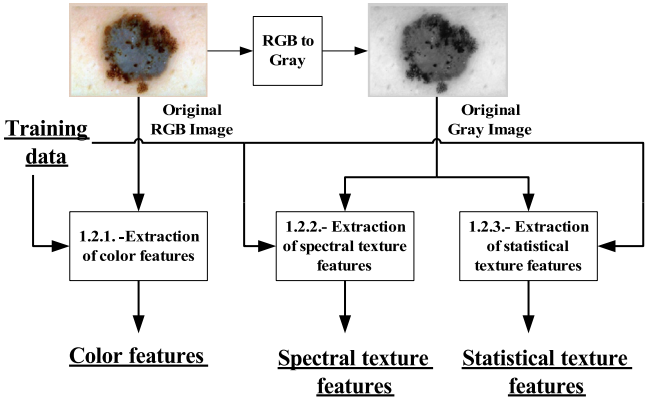

Fig. 5. Design of Sub-block 1.2. – Extraction of features.

For the transformation of the RGB image to the gray scale, the usual formula was used [47]:

$$I_G(x,y) = 0.2989 I_{RGB}(x,y,0) + 0.587 I_{RGB}(x,y,1) + 0.114 I_{RGB}(x,y,2) \quad (1)$$

Sub-block 1.2.1. – *Extraction of color features*: From the RGB image different color features were extracted with the aim of characterizing the color of the pixels in the reticular structure. To this purpose, various color spaces were used: RGB, rgb (RGB normalized), HSV, CIEXYZ, CIELab and CIELuv [47], choosing as features the values of the channels.

As can be consulted in [48,15], the HSV and the CIELuv spaces have the property of being decoupled the chrominance and the luminance and the rgb and the HSV spaces (the H and S channels) have the property of being invariants to illumination intensity. Both properties are important criteria for dealing with images which are acquired in uncontrolled imaging conditions.

To avoid the noise, for each pixel the color features were calculated in the pixels of its 5×5 neighborhood, obtaining subsequently the median of the values.

Sub-block 1.2.2. – *Extraction of spectral texture features*: In Fig. 6 the design of the spectral texture features extraction can be observed graphically. In the first place, a bank of Gaussian filters is applied over the gray image, obtaining a set of blurred images for $\sigma = 1, 2, \ldots \sigma_{max}$. Secondly, both over the original gray image and blurred images the extraction of the Sobel and Hessian features is carried out. Thirdly, from the blurred images are extracted the Gaussian and DoG features.

Bank of Gaussian filters $\sigma = 1, 2, 4, \ldots, \sigma_{max}$: Previous to the obtaining of spectral features, as it can be seen in Fig. 6, a bank of Gaussian filters [47] is applied over the gray image for the values $\sigma = 1, 2, 4, \ldots, \sigma_{max}$ where σ_{max} is a threshold value, being the σ values of the form: $\sigma = 2^m$, with $m = 0, 1, 2, \ldots, m_{max}$ and m_{max} in such a way that $\sigma_{max} = 2^{m_{max}}$. Hence, the next formula is applied over the image, for each σ value:

$$G_\sigma(x,y) = \frac{1}{2\pi\sigma^2} e^{-(x^2+y^2)/2\sigma^2} \quad (2)$$

where (x,y) are the spatial coordinates.

The motivation to carry out this filtering is, on the one hand, to eliminate part of the existing noise and, on the other hand, to characterize the neighborhood of reticular pixels through the conjunction of this filtering together with the subsequent extraction of spectral features, for the different values of σ.

The threshold values established for the values of the resolutions and magnifications of images in the dataset employed in this work are $\sigma_{max} = 8$ and $m_{max} = 3$.

Extraction of Sobel features: As can be seen in Fig. 6, the Sobel features are extracted from both the original gray image and the

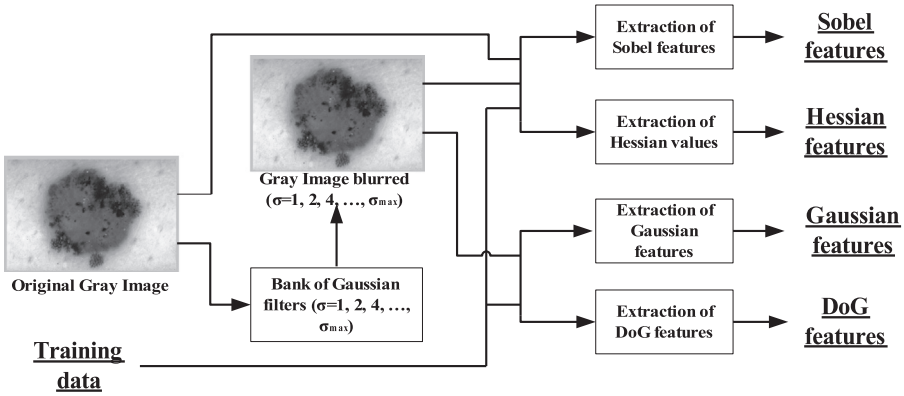

Fig. 6. Design of Sub-block 1.2.2. – Extraction of spectral texture features.

blurred images, for $\sigma = 1, 2, 4, \ldots, \sigma_{max}$. To achieve this, the Sobel operator [47] is applied over the different images and the features are extracted thereupon. The Sobel operator is commonly used for edge detection, because it gives the magnitude of the largest possible change, its direction and the direction from dark to light. There were chosen as features in the corresponding pixels of the convolved images the next values of the gradient: the *module* and the *direction*.

Extraction of Hessian features: The Hessian features [47] are extracted from both the original gray image and the blurred images, for $\sigma = 1, 2, 4, \ldots, \sigma_{max}$, as shown in Fig. 6. For this purpose, for each image, the Hessian matrix is calculated in the first place:

$$H(x,y) = \begin{pmatrix} D_{xx}(x,y) & D_{xy}(x,y) \\ D_{yx}(x,y) & D_{yy}(x,y) \end{pmatrix} \quad (3)$$

where (x, y) are the spatial coordinates and D_{xx}, D_{xy}, D_{yx} and D_{yy} are the second order partial derivatives in *xx*, *xy*, *yx* and *yy* directions.

Subsequently, there were chosen as features in the corresponding pixels of the convolved images the next values calculated over the Hessian matrix: the *determinant* (DoH: "Determinant of Hessian"), the *trace* and the *module* ($module = \sqrt{(D_{xx})^2 + D_{xy}.D_{yx} + (D_{yy})^2}$), relevant values in the characterization of the texture.

Extraction of Gaussian features: In the previous stage, for the different values $\sigma = 1, 2, 4, \ldots, \sigma_{max}$ different Gaussian filters were applied, as shown in Fig. 6. The process of extraction of Gaussian features simply consists in the extraction of the pixel values in the different blurred images for each σ.

Extraction of DoG features: As can be seen in Fig. 6, the DoG ("Difference of Gaussians") features are extracted from the blurred images, for $\sigma = 1, 2, 4, \ldots, \sigma_{max}$. To this end, the DoG filter is applied, in which, for the different pairs of values (σ_i, σ_j), such as $i > j$ and $\sigma_k = 2^k$, with $k = 0, 1, \ldots, m_{max}$, the following formula is applied:

$$DoG_{\sigma_i \sigma_j}(x,y) = G_{\sigma_i}(x,y) - G_{\sigma_j}(x,y) \quad (4)$$

where (x, y) are the spatial coordinates and $G_{\sigma_i}(x,y)$ and $G_{\sigma_j}(x,y)$ are the Gaussian filters of the bank, applied over the gray image, previously calculated, corresponding to σ_i and σ_j values respectively.

The DoG is a low-pass filter used to increase the visibility of edges and other details presented in a digital image. There were chosen as features, the pixel values in the different convolved images, for each (σ_i, σ_j).

Sub-block 1.2.3. – *Extraction of statistical texture features*: From the gray image, the extraction of statistical texture features has been performed using GLCM ("Gray Level Co-occurrence Matrix") technique [49], widely used with good results in the characterization of the texture.

To quantify the texture in the $n \times n$ neighborhoods of the pixels, for each one of the values $n = 1, 3, \ldots, n_{max}$, being n_{max} a threshold value, the normalized GLCM matrices were obtained and over these matrixes the following statistics were also calculated and chosen as features: *variance* and *entropy*. These are two of the most relevant ones among the 14 commonly used [50], being moreover the *entropy* robust to linear shifts in the illumination intensity [51]. In order to achieve an invariance with respect to the rotation, GLCM was calculated in each one of the directions $\{0°, 45°, 90°, 135°\}$ and the statistics calculated from these matrices were averaged.

The threshold value established for the values of the resolutions and magnifications of images in the dataset employed in this work is $n_{max} = 7$.

Sub-block 1.3. – *Analysis of data*: Once the extraction of features is done, the analysis of data is carried out. For this purpose, the C4.5 [52] method is used. It is a method developed by Ross Quinlan for building decision trees by means of training data, widely used in recent years with good results.

In this work the J48 implementation of the C4.5 algorithm has been used. J48 is part of the Weka library [53]. For the machine learning process the same configuration of [26] was used, focusing on the next parameters for the modeling: the confidence factor (C) and the minimum number of samples per leaf (M). There were set the values at 0.1 and 100.

Over these samples the values of the color, spectral and statistical features were extracted, up to a total number of 80 features per sample. By means of the training data, a decision tree classifier was generated, implementing the rules corresponding to the pixels candidates to be part of the pigment network.

There were selected 23 features, 17 of texture and 6 of color. The most relevant features in the tree were the DoH ("Determinant of Hessian"), for $\sigma = 4$, and the DoG ("Difference of Gaussians"), for $\sigma = 8$. Between the color features, the most relevant feature was the b channel of the rgb (RGB normalized) space.

The model was over 90% accurate, which is a good illustration of the obtained results. This issue will be further discussed in the results section, explaining the results obtained.

Sub-block 1.4. – *Applying machine learning generated rules*: By means of the original image and the generated rules implemented by the decision tree classifier, an iterative process over all the pixels is carried out in the image and the mask corresponding to the pixels candidates to be part of the pigment network is obtained.

Fig. 7 provides four examples that illustrate the application of this process in dermoscopic images. As can be observed, there are three cases of images containing the reticular pattern and a fourth one without. From those images, the masks with the candidate pixels are obtained as a result of the application of the generated rules. In the case of the first three, the vast majority of the pixels that are part of the reticular structure were selected, although some not belonging to this structure were also selected, being noise of the masks; for example, in the third example the pixels of the hairs have been selected. In the case of the fourth one there are also many selected pixels that clearly has no reticular pattern.

It therefore becomes evident that there is a need for a structural analysis over the mask with the pixels candidates, with the aim of detecting reticular structures. This process is described in the next section.

3.2.2. Block 2: Detection of the pigment network structure

In the previous block the mask with the pixels candidates to be part of the pigment network has been obtained. In this block, a reticular structure detection process is conducted, with the aim of undertaking the diagnosis, that is to say, whether it has pigment network or not, and also obtaining the mask corresponding to this pattern, if any.

In Fig. 8 the graphical design of this process can be seen. As shown, the process of detecting the pigment network structure consists of four stages: in the first stage, the 8-connected components higher than a given value are obtained; in the second stage, each one of them is iterated, determining whether it has a reticular structure and also calculating the number of holes; in the third stage, the diagnosis is carried out; finally, in the fourth stage, in positive case, the mask of the pigment network is generated.

Furthermore, in this block five thresholds to be parameterized depending on different resolutions and magnifications are specified: $numHolesSubmask_{min}$, $percentHolesSubmask_{min}$, $numHolesTotal_{min}$, $numPixelsSubRegion_{min}$ and $numPixelsHole_{min}$. The values of these thresholds for the used dataset were obtained empirically.

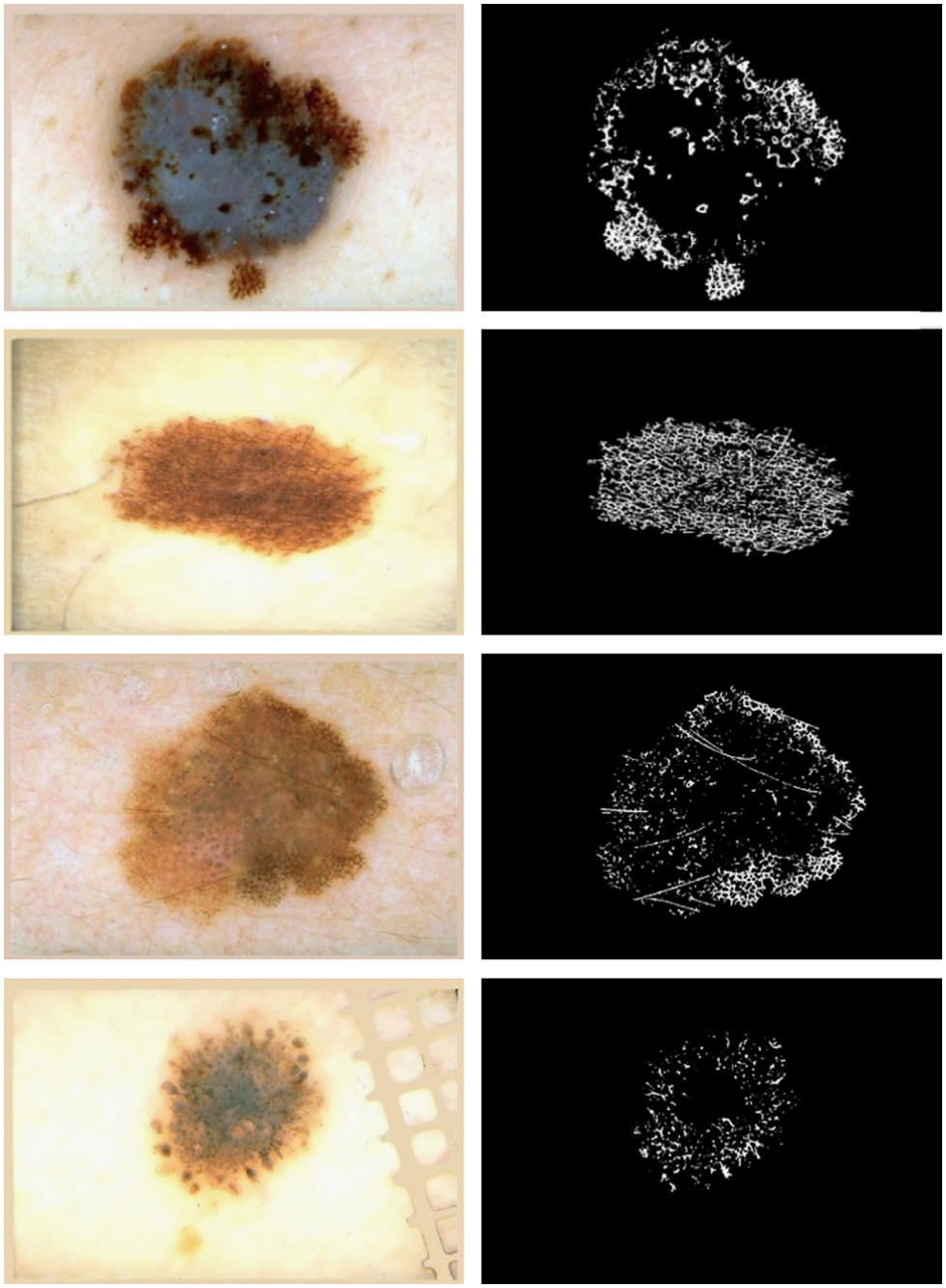

Fig. 7. Four examples of the execution of the machine learning process. On the left the original images and on the right the masks with the images candidate to be part of the pigment network. The first three have a reticular pattern, whereas the fourth one does not.

Additionally, it should be noted that this method arranges the possible noise generated by different artifacts not previously pre-processed. One relevant case is the detection as reticular of the pixels of a hair by means of the generated rules, something that is fixed in this step, since it is a structure without holes, lacking a net shape.

Sub-block 2.1. – *Obtaining 8-connected sub-masks greater than a minimum value*: As can be seen in Fig. 8, the mask with the candidate pixels is taken as input value. By means of this, the 8-connected components $C_1, C_2, \ldots, C_L$ are obtained.

Subsequently, it is iterated over each one of the components calculating its area, and those having an area higher than a threshold area $numPixelsSubRegion_{min}$ are selected, that is to say, there are obtained the M components $C_1, C_2, \ldots, C_M$, with $M <= L$ which fulfill the condition $(Area(C_i) >= numPixelsSubRegion_{min})$ for $i = 1, 2, \ldots, M$.

The threshold value employed in this study is $numPixelsSubRegion_{min} = 100$.

Sub-block 2.2. – *Determining C_i has pigment network shape* $(i = 1, 2, \ldots, M)$: As shown in Fig. 8, C_i for $i = 1, 2, \ldots, M$ from the previous stage are taken as input values, and as output values the different C_i and $numH_i$, for $i = 1, 2, \ldots, N$ are taken, the C_i being the sub-regions that have pigment network shape and the $numH_i$ the number of holes contained in each one, for the different i values $i = 1, 2, \ldots, N$. Obviously, $N <= M$ is given.

This process is decomposed into 4 steps, for each C_i $(i = 1, 2, \ldots, M)$, as it is shown in Fig. 9. In the first place the complement of the sub-region is calculated; secondly, the holes are obtained; thirdly, by means of the previous information, the values used as a criteria to determine whether it has pigment network shape are extracted; finally, in fourth place, such criteria are

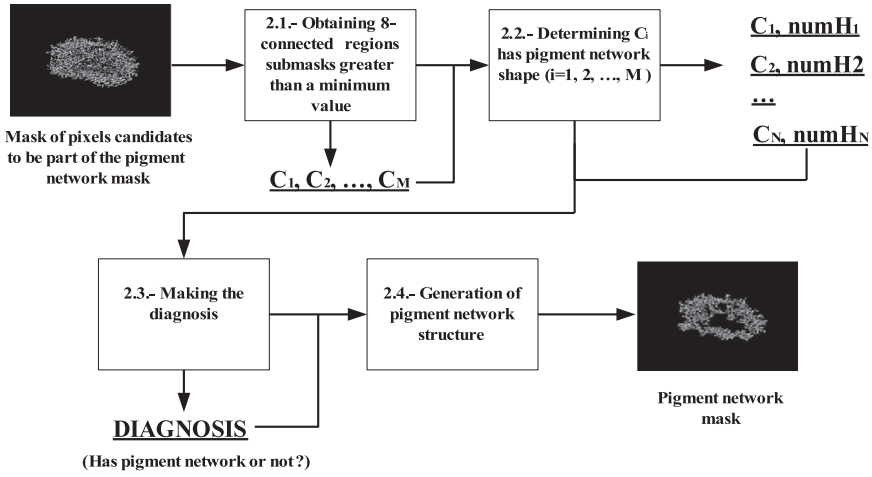

Fig. 8. Design of Block 2. – Detection of the pigment network structure.

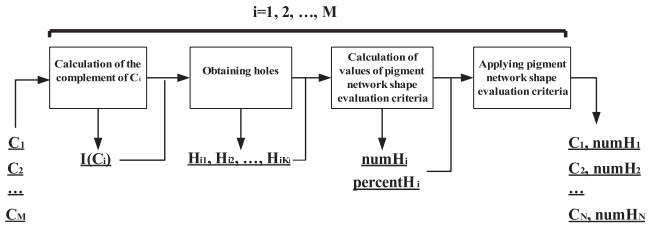

Fig. 9. Design of Sub-block 2.2. – Determining C_i has pigment network shape $i = 1, 2, \ldots, M$.

applied to C_i, also obtaining the number of $numH_i$ holes. These steps will now be explained in detail.

Calculation of the complement of C_i: In this step, the complement of the C_i is calculated: $I(C_i)$, aimed at obtaining which part of the sub-mask corresponds to the background of the lesion from which the subsequent extraction of the holes will be conducted.

Obtaining holes: In the first place, from $I(C_i)$, the *Ri*8-connected components of the mask which do not touch the image border are obtained: $H_1, H_2, \ldots, H_{R_i}$, corresponding to the holes of C_i.

Secondly, from these holes of C_i, those H_j $(j = 1, 2, \ldots, K_i)$ fulfilling the condition $(numPixelsHole_{min} <= Area(H_j))$ are selected, where $numPixelsHole_{min}$ is a threshold value. Obviously, $K_i <= R_i$ is given.

The threshold value employed in this study is $numPixelsHole_{min} = 20$.

Calculation of values of pigment network shape evaluation criteria: In this step the criteria used to evaluate whether the C_i sub-region has a pigment network shape is calculated.

In the first place, $H_i = \bigcup_{j=1}^{j=K_i} H_j$ is calculated.

Secondly, two indicator values for the evaluation of the shape, $numH_i$ and $percentH_i$ are obtained. The first corresponds to the number of holes of C_i fulfilling the conditions (obtained in the previous stage): $numH_i = K_i$, and the second one to the percentage of the area between the union of all the holes in the C_i component: $percentH_i = Area(H_i)/Area(C_i)$.

Applying pigment network shape evaluation criteria: In this case, the criteria to evaluate whether the C_i subregion has the proper shape are applied by analyzing the values of $numH_i$ and $percentH_i$.

C_i is considered part of a reticular structure if the next two conditions are met:

$(numH_i >= numHolesSubmask_{min})$ and $(percentH_i >= percentHolesSubmask_{min})$ where $numHolesSubmask_{min}$ and $percentHolesSubmask_{min}$ are threshold values.

The threshold values employed in this work are $numHolesSubmask_{min} = 3$ and $percentHolesSubmask_{min} = 0.04$.

As a result of this last stage, it is calculated whether C_i has a reticular structure (and therefore whether it is part of the pigment network mask) and its number of holes: $numH_i$.

Therefore, in this sub-block N sub-regions are selected and the obtained values enable the diagnosis, whether it has pigment network or not, in the next sub-block.

Sub-block 2.3. – *Making the diagnosis*: As shown in Fig. 8, by means of the C_i and $numH_i$ obtained for $i = 1, 2, \ldots, N$ in the previous stage, the diagnosis is carried out. This is done in two steps.

Firstly, the total number of holes is calculated, as follows: $numHolesTotal = \sum_{i=1}^{N} numH_i$.

Secondly, the diagnosis is carried out, that is to say, it is determined whether the mask has a reticular structure or not. The criteria used to do so is the condition: $(numHolesTotal >= numHolesTotal_{min})$, where $numHolesTotal_{min}$ is a threshold value.

The threshold value employed in this work is $numHolesTotal_{min} = 5$.

Sub-block 2.4. – *Generation of pigment network structure*: As can be seen in Fig. 8, by means of the diagnosis and the sub-masks C_i for $i = 1, 2, \ldots, N$, obtained in the previous sub-blocks, the mask of the pigment network is generated.

Obviously, if the diagnosis is negative, the resulting mask will be empty. In affirmative case, the mask PN of the pigment network will be calculated as $PN = \bigcup_{i=1}^{i=N} C_i$.

In Fig. 10, four examples are displayed. These four examples are the same as those ones in Fig. 7. As can be observed, in the first three cases, the mask of the candidate pixels is processed and as a result the noise is reduced and the reticular mask is obtained, having in the third one an example of how distortive artifacts are eliminated in this structural analysis process. In the fourth case, where the mask of the candidate pixels has a clearly non-reticular structure, all the pixels are discarded, obtaining a non-reticular diagnosis.

4. Results

The reliability of the method was tested by analyzing the results obtained over the image database, created with the collaboration of J.L. Diaz and J. Gardeazabal, dermatologists from Cruces Hospital in Bilbao, Spain. It consists of 220 images, with a resolution of 768×512 and $10\times$ magnification, having 120 without a reticular structure and 100 with such structure. All the images were catalogued by the dermatologists.

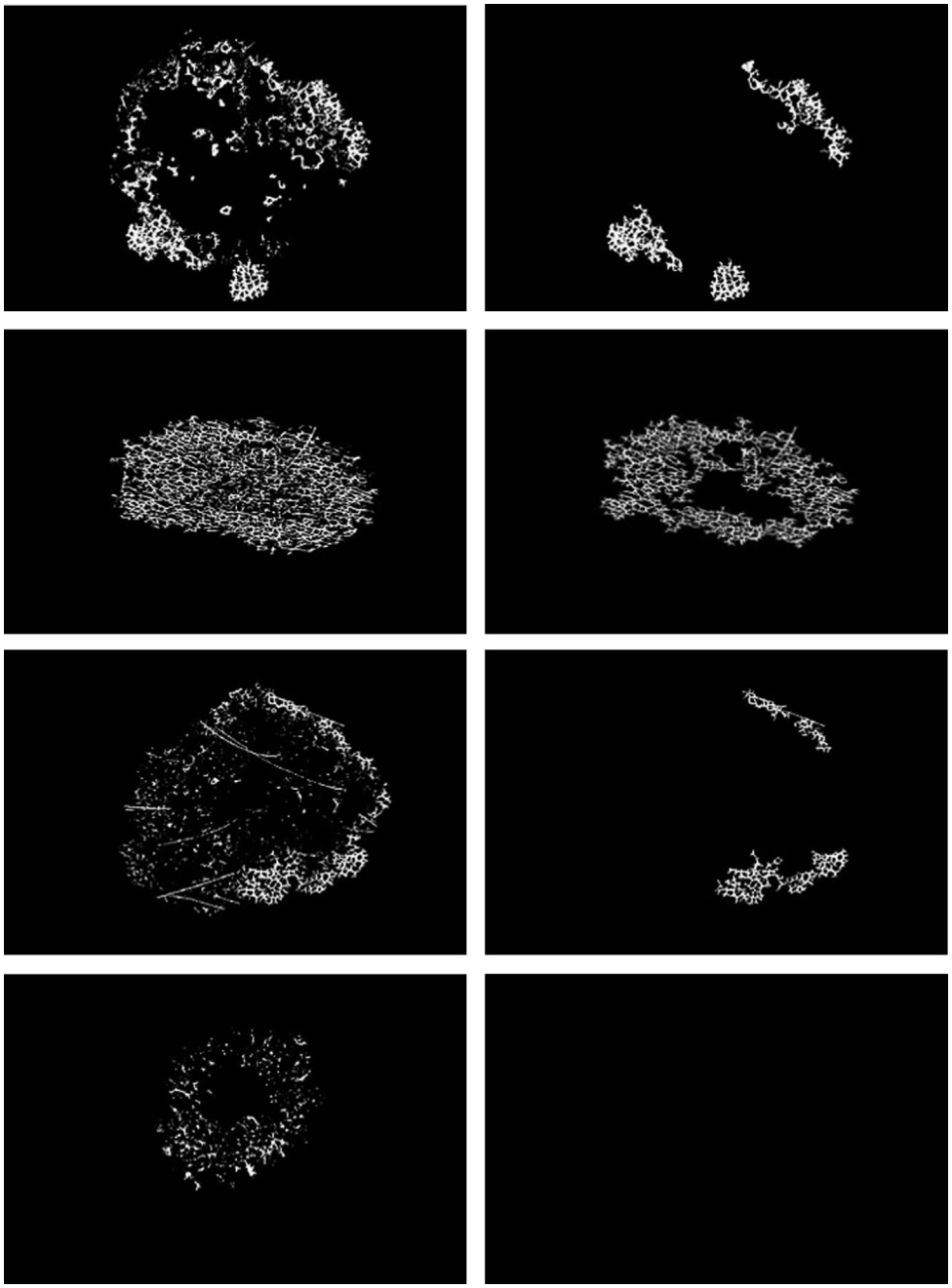

Fig. 10. Four examples of the execution of the reticular structure detection process through the mask with the candidate pixels. The four examples are the same as in Fig. 7, in which some examples of the result of the machine learning process are shown. The first three have a reticular pattern, whereas the fourth one does not.

The results are displayed below, showing in the first place the results of the first block, corresponding to the supervised machine learning process, and secondly the results after finishing the second block corresponding to the detection of the reticular pattern structure, which really are the results of the overall method.

4.1. Supervised machine learning results

As stated above, a total number of 40 images were selected, 25 of them with the reticular pattern. Over these images, with the help of the two expert dermatologists mentioned above, there were selected different samples of reticular and non-reticular pixels, up to a total of 400 for each case, thus obtaining a total number of 800 different samples.

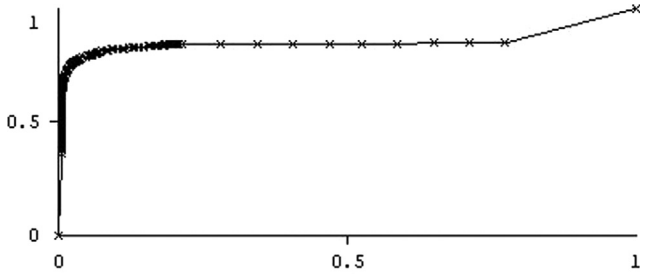

Fig. 11. ROC of the supervised machine learning process.

Over these samples the values of the color, spectral and statistical features were extracted, up to a total number of 80 features per sample. The model was created using the C4.5 algorithm for the

generation of a decision tree classifier, which implements the rules for the classification of the pixels of the image between "reticular" and "non-reticular". In Fig. 11 the ROC ("Receiver Operating Characteristic") curve corresponding to the classification model obtained in the supervised machine learning process is displayed.

The AUC ("Area Under Curve") of the ROC obtained in the model for the detection of pixels candidates to be part of the reticular pattern, by means of the training data, was 0.90, which is a good measurement of the reliability of the employed method. Over such ROC curve it was selected as optimal value a point with a sensitivity of 92% and a specificity of 90%.

4.2. Results of the overall method

The method was tested against the image database which, as stated before, consists of 220 images, 120 without a reticular structure and 100 with. In the evaluation of the results of the whole method TP, FP, TN and FN were defined as follows:

TP: Images WITH reticular patter. Result of the diagnosis: YES
FP: Images WITHOUT reticular pattern. Result of the diagnosis: YES
TN: Images WITHOUT reticular pattern. Result of the diagnosis: NO
FN: Images WITH reticular pattern. Result of the diagnosis: NO

Some examples of the results of the algorithm are displayed below. In Fig. 12 four cases of TP are presented, in Fig. 13 four cases of TN, in Fig. 14 two cases of FN and, finally, in Fig. 15 two cases of FP are presented.

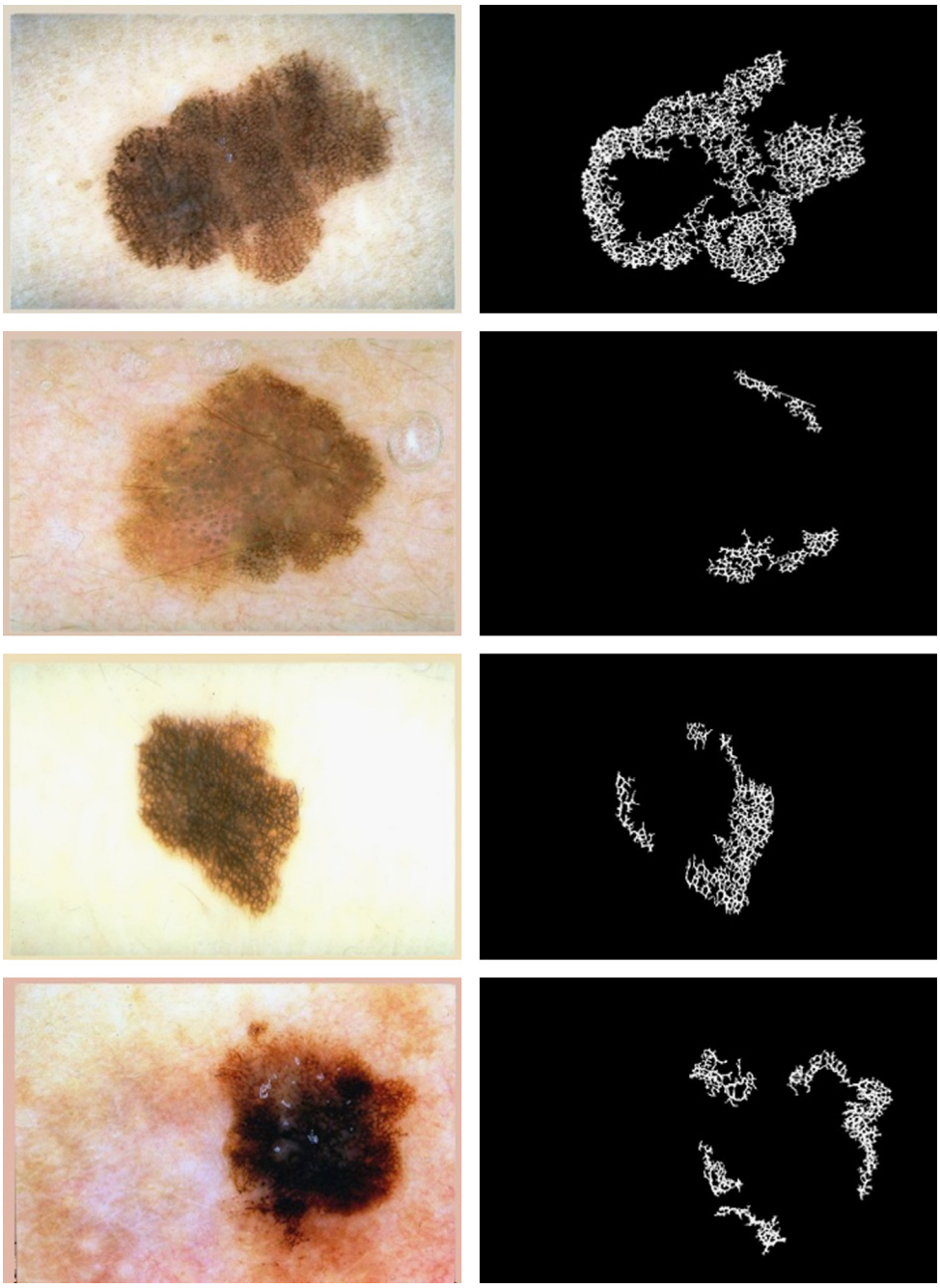

Fig. 12. Four examples of TP.

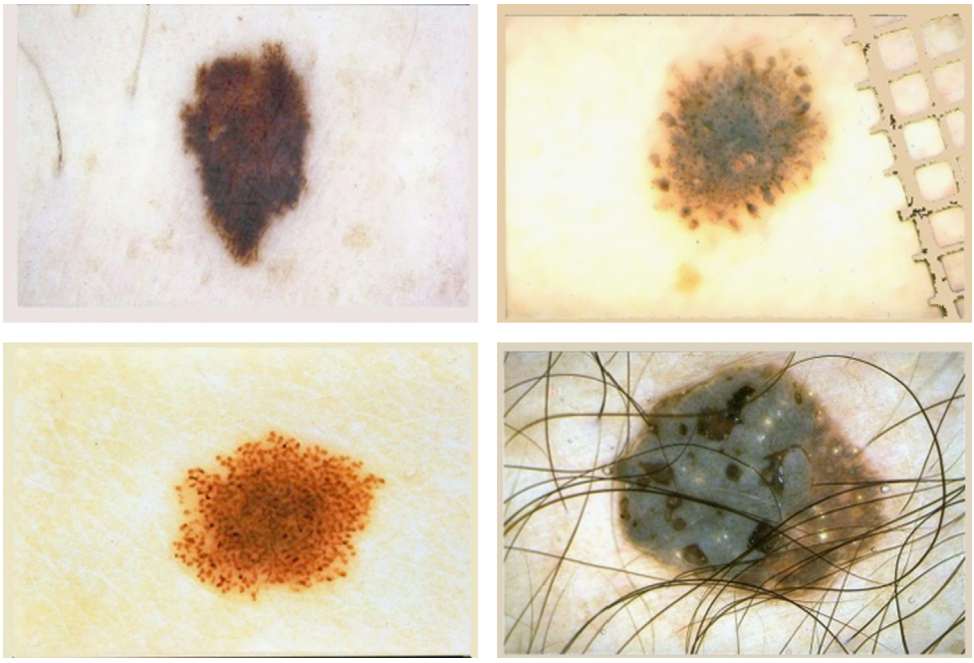

Fig. 13. Four examples of TN. In the fourth image it can be seen how the process does not fail in those cases where there is a high number of hairs.

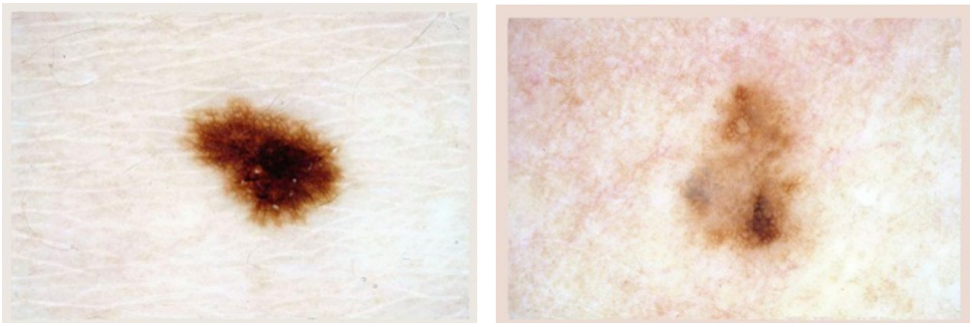

Fig. 14. Two examples of FN. In both cases the reticular structures are very faint.

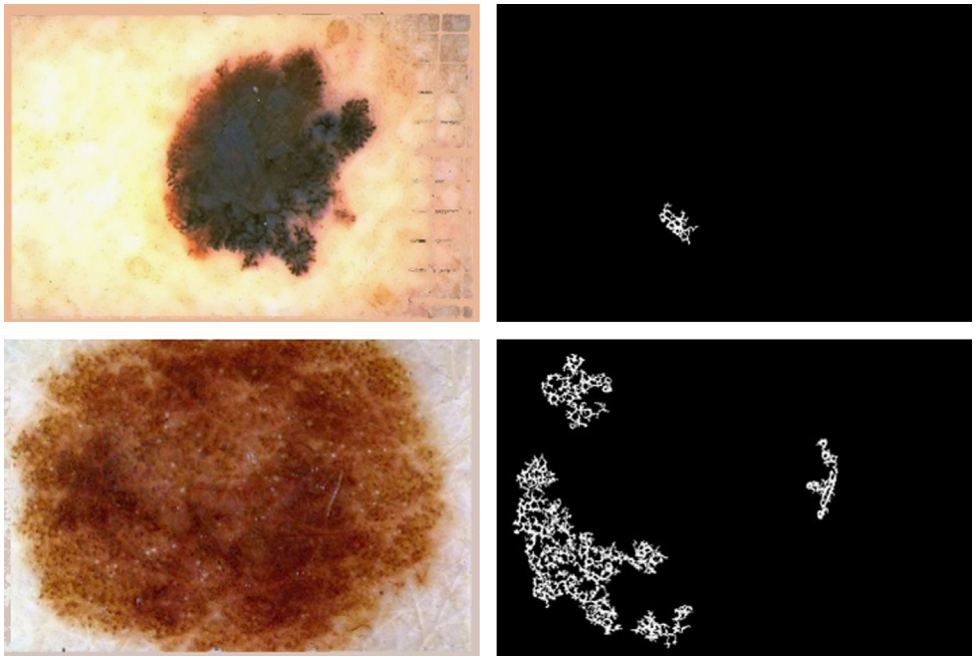

Fig. 15. Two examples of FP. In both cases there is a great number of pixels together with a texture similar to the reticular one.

Table 1
Results of the test with all the database images.

Pattern	Positive	Negative
Reticular	86 (TP)	14 (FN)
Non reticular	22 (FP)	98 (TN)

Table 2
Results of the most relevant works in the detection of pigment network (ACC: accuracy, SE: sensitivity, SP: specificity).

Work	# Images	Results
Anantha et al. [37]	155	80% ACC
Sadeghi et al. [43]	436	93.30% ACC
Gola et al. [25]	40	100% SE – 92.86% SP
Barata et al. [46]	200	91.1% SE – 82.1% SP
García et al. (Proposed)	220	86% SE – 81.67% SP

The results of the proposed algorithm in Table 1.

Hence, the algorithm has very encouraging and clearly reliable overall results, with 83.64% in accuracy.

As regards sensitivity, a ratio of 86% was obtained, thus detecting the reticular pattern in an accurate manner, as can be observed in Fig. 12. The majority of cases in which it fails occur when the reticular structures are very tenuous, as can be seen in Fig. 14.

As regards specificity, it works in 81.67% of the cases, identifying the absence of the reticular pattern, as can be seen in Fig. 13, even when there is a high number of hairs. The case in which it fails is in the images where there are many pixels together with a texture similar to the reticular one, which cannot be screened by the structural analysis process, as can be seen in Fig. 15.

The comparison with the methods of the state of the art is very difficult. In the first place, in some of them no result is presented; in other ones some outcomes are presented, but their aims are different from the ones in this work, which is focused on the differentiation between “Pigment network” and “No pigment network”. From the studies reported in the state of the art, this could be the case of [36,39,29,40,41,44,45]. Secondly, even in the case of studies that present reticular pattern detection outcomes, a real comparison cannot be carried out, since all of them use different databases. It is a serious problem faced by research groups in the automated detection of melanoma. There are several public dermoscopy atlases like [54], which can be purchased by research groups, that select the images to be analysed, conducting a classification and labelling process over them, building the final datasets for the design, implementation and testing of their methods. But these ones are not public, so there is no public database, against which the robustness of the algorithms developed by the different research groups can be compared.

In any case, by way of illustration the results of out work against the works of the state of the art which present results in the differentiation between “Pigment network” and “No pigment network” are presented in Table 2.

As can be seen, the proposed work offer good results, comparing with other ones. Anyway, it should be taken into account the above comments.

5. Discussion

A robust algorithm showing good results for the detection of the reticular pattern has been presented.

As has been indicated before, the reticular pattern was successfully detected in the images with pigment network in 86% of the cases. Most of the errors occurred in images in which this pattern was presented in a tenuous or unclear way, being the origin of those failures in the supervised machine learning process, due to the fact that, with the generated rules, most of the reticular pixels in which there was a low contrast between the net and the background were not detected properly. Some attempts were made to increase the sensitivity by modifying the machine learning process, but this resulted in a lowering of specificity. With a view to improving this aspect, in future studies the machine learning process will be enhanced by adding new samples and features.

Conversely, in the case of the images not containing a reticular pattern, there is success in 81.67% of the cases. Most cases in which this occurs are when there is a high number of pixels together, with a texture similar to the reticular one, especially when they are grouped and form structures with holes. The origin of those failures was, as in the previous case, in the supervised machine learning process, and was also attempted to increase specificity by modifying this process, but again that involved decreasing of sensitivity. Thus it was concluded that, as above, in order to improve this aspect the machine learning process should be improved in future studies.

For the reproducibility of the algorithm in another database, with other resolution and magnification values, the parameterization of the thresholds depending on them will be needed σ_{max} (and its corresponding m_{max}) and n_{max} for the block 1 of the algorithm and $numHolesSubmask_{min}$, $percentHolesSubmask_{min}$, $numHolesTotal_{min}$, $numPixelsSubRegion_{min}$ and $numPixelsHole_{min}$ for the block 2 of the algorithm, as commented before.

In this study, the two threshold values of the first block (σ_{max} set to 8 and its corresponding m_{max} set to 3 and n_{max} set to 7) have been chosen from the beginning, in the feature extraction, since it has been considered that, given the resolution and magnification of the used images and the texture of the pixels of the pigment network, enabled sufficient ranges. In the case of the five threshold values of the second block, the setting was done empirically, in four steps. In the first place, $numPixelsSubRegion_{min}$ was set to 100. Secondly, $numPixelsHole_{min}$ was set to 20. In the third place, $numHolesSubmask_{min}$ and $percentHolesSubmask_{min}$ were set to 3 and 0.04 respectively. Finally, $numPixelsHole_{min}$ was set to 5. In all the steps several values were tested, selecting the best ones.

Another point to be borne in mind is that, as stated before, with the design chosen in the algorithm, there is no need to carry out preprocessing and segmentation prior to the detection of pigment network. Artifacts such as bubbles, rules or hairs are discarded by the algorithm, either in the first block, discarding most of the pixels, or in the second block, removing all the structures corresponding to the artifacts.

Finally, it is important to emphasize here that the main aim of the presented algorithm is to diagnose whether the image has pigment network or not, the precise segmentation of the corresponding mask being secondary. This is a matter of importance, since in the design of the algorithm, to ensure reliability in the reticular diagnosis, it does not matter to lose a part of the reticular mask, with the aim of increasing the specificity (not taking as reticular those other images that are not) or, conversely, to have pieces of reticular from pixels that do not actually belong to that pattern, with the aim of increasing the sensitivity (not taking as not reticular those other images that actually are).

6. Conclusions and future work

An algorithm for detection of the reticular pattern over dermoscopic images has been presented, consisting of two blocks. In the first one a supervised machine learning process is carried out

generating a set of rules that, when applied to the image, allow obtaining a mask with the pixels candidates to be part of the pigment network. In the second one, this mask is processed conducting a structural analysis process in which the reticular pattern is pursued, aimed at obtaining the diagnosis, that is to say, whether it has pigment network or not, and to generate the mask corresponding to that structure, if any.

It has a high degree of reliability, thus obtaining encouraging results: 83.64% accuracy, 86% sensitivity and 81.67% specificity. It is an algorithm with an innovative design that can be applied to the original image (without the need of conducting previous preprocessing and segmentation), robust against the presence of distortive artifacts, which is designed in a scalable way (the improvements and extensions are easy to undertake) and, finally, parameterized regarding its use with images of different resolutions and magnifications.

Notwithstanding, work is going on the improvement of the algorithm, especially in the supervised machine learning process. Additionally, further work is underway on the extension of the algorithm in order to widen its scope to the differentiation between typical and atypical, and also to incorporating the detection of new dermoscopic structures, such as globules, dots and streaks.

Conflict of interest statement

None declared.

Acknowledgment

This research was partially supported by the Basque Government Department of Education (eVIDA Certified Group IT579-13).

References

[1] World Cancer Research Fund International, Cancer statistics—Worldwide, 2008, http://www.wcrf.org/cancer_statistics/world_cancer_statistics.php (Online accessed 10-Oct-2013).
[2] Skin Cancer Foundation, Skin cancer facts, 2013, http://www.skincancer.org/Skin-Cancer-Facts/ (Online accessed 10-Oct-2013).
[3] J. Malvehy, S. Puig, G. Argenziano, A.A. Marghoob, H.P. Soyer, Dermoscopy report: proposal for standardization. Results of a consensus meeting of the International Dermoscopy Society, J. Am. Acad. Dermatol. 57 (2007) 84–95.
[4] E.L. Psaty, A.C. Halpern, Current and emerging technologies in melanoma diagnosis: the state of the art, Clin. Dermatol. 27 (2009) 35–45.
[5] D.S. Rigel, J. Russak, R. Friedman, The evolution of melanoma diagnosis: 25 years beyond the ABCDs, CA: Can. J. Clin. 60 (2010) 301–316.
[6] L. Smith, S. Macneil, State of the art in non-invasive imaging of cutaneous melanoma, Skin Res. Technol. 17 (2011) 257–269.
[7] A.G. Goodson, D. Grossman, Strategies for early melanoma detection: approaches to the patient with nevi, J. Am. Acad. Dermatol. 60 (2009) 719–738.
[8] P. Guitera, S.W. Menzies, State of the art of diagnostic technology for early-stage melanoma, Expert Rev. Antican. Ther. 11 (2011) 715–723.
[9] H. Pehamberger, A. Steiner, K. Wolff, In vivo epiluminescence microscopy of pigmented skin lesions. I. Pattern analysis of pigmented skin lesions, J. Am. Acad. Dermatol. 17 (1987) 571–583.
[10] W. Stolz, A. Riemann, A. Cognetta, ABCD rule of dermatoscopy: a new practical method for early recognition of malignant melanoma, Eur. J. Dermatol. 4 (1994) 521–527.
[11] S.W. Menzies, C. Ingvar, K.A. Crotty, W.H. McCarthy, Frequency and morphologic characteristics of invasive melanomas lacking specific surface microscopic features, Arch. Dermatol. 132 (1996) 1178–1182.
[12] G. Argenziano, G. Fabbrocini, P. Carli, V. De Giorgi, E. Sammarco, M. Delfino, Epiluminescence microscopy for the diagnosis of doubtful melanocytic skin lesions. Comparison of the ABCD rule of dermatoscopy and a new7-point checklist based on pattern analysis, Arch. Dermatol. 134 (1998) 1563–1570.
[13] K. Korotkov, R. Garcia, Computerized analysis of pigmented skin lesions: a review, Artif. Intell. Med. 56 (2012) 69–90.
[14] H. Ganster, A. Pinz, R. Röhrer, E. Wildling, M. Binder, H. Kittler, Automated melanoma recognition, IEEE Trans. Med. Imaging 20 (2001) 233–239.
[15] M.E. Celebi, H.A. Kingravi, B. Uddin, H. Iyatomi, Y.A. Aslandogan, W.V. Stoecker, R.H. Moss, A methodological approach to the classification of dermoscopy images, Comput. Med. Imaging Graph. 31 (2007) 362–373.
[16] H. Iyatomi, H. Oka, M.E. Celebi, M. Hashimoto, M. Hagiwara, M. Tanaka, K. Ogawa, An improved Internet-based melanoma screening system with dermatologist-like tumor area extraction algorithm, Comput. Med. Imaging Graph. 32 (2008) 566–579.
[17] J. Fernandez Alcon, C. Ciuhu, W. Ten Kate, A. Heinrich, N. Uzunbajakava, G. Krekels, D. Siem, G. De Haan, Automatic imaging system with decision support for inspection of pigmented skin lesions and melanoma diagnosis, IEEE J. Sel. Topics Signal Process. 3 (2009) 14–25.
[18] G. Di Leo, A. Paolillo, P. Sommella, G. Fabbrocini, Automatic diagnosis of melanoma: a software system based on the 7-point check-list, in: 2010 43rd Hawaii International Conference on System Sciences, IEEE, 2010, pp. 1–10.
[19] J.L. García Arroyo, B. García Zapirain, Automated detection of melanoma in dermoscopic images, in: Computer Vision Techniques for the Diagnosis of Skin Cancer, Springer, 2013, pp. 1–55.
[20] H. Mirzaalian, T.K. Lee, G. Hamarneh, Learning features for streak detection in dermoscopic color images using localized radial flux of principal intensity curvature, in: 2012 IEEE Workshop on Mathematical Methods in Biomedical Image Analysis, IEEE, 2012, pp. 97–101.
[21] M. Sadeghi, T.K. Lee, D. Mclean, H. Lui, M.S. Atkins, Oriented pattern analysis for streak detection in dermoscopy images, in: Medical Image Computing and Computer-Assisted Intervention-MICCAI 2012, pp. 298–306.
[22] M. Sadeghi, T. Lee, H. Lui, D. McLean, S. Atkins, Detection and analysis of irregular streaks in dermoscopic images of skin lesions, IEEE Trans. Med. Imaging (2013).
[23] S. Yoshino, T. Tanaka, M. Tanaka, H. Oka, Application of morphology for detection of Dots in tumor, in: SICE 2004 Annual Conference, vol. 1, 2004, pp. 591–594.
[24] J. Xu, K. Gupta, W.V. Stoecker, Y. Krishnamurthy, H.S. Rabinovitz, A. Bangert, D. Calcara, M. Oliviero, J.M. Malters, R. Drugge, R.J. Stanley, R.H. Moss, M.E. Celebi, Analysis of globule types in malignant melanoma, Arch. Dermatol. 145 (2009) 1245–1251.
[25] A. Gola Isasi, B. García Zapirain, A. Méndez Zorrilla, Melanomas non-invasive diagnosis application based on the ABCD rule and pattern recognition image processing algorithms, Comput. Biol. Med. 41 (2011) 742–755.
[26] M.E. Celebi, H. Iyatomi, W.V. Stoecker, R.H. Moss, H.S. Rabinovitz, G. Argenziano, H.P. Soyer, Automatic detection of blue-white veil and related structures in dermoscopy images, Comput. Med. Imaging Graph. 32 (2008) 670–677.
[27] G. Di Leo, G. Fabbrocini, A. Paolillo, O. Rescigno, P. Sommella, Towards an automatic diagnosis system for skin lesions: estimation of blue-whitish veil and regression structures, in: 2009 6th International Multi-Conference on Systems, Signals and Devices, IEEE, 2009, pp. 1–6.
[28] J.L. García Arroyo, B. García Zapirain, A. Mendez Zorrilla, Blue-white veil and dark-red patch of pigment pattern recognition in dermoscopic images using machine-learning techniques, in: 2011 IEEE International Symposium on Signal Processing and Information Technology (ISSPIT), IEEE, 2011, pp. 196–201.
[29] G. Betta, G. Di Leo, G. Fabbrocini, A. Paolillo, P. Sommella, Dermoscopic image-analysis system: estimation of atypical pigment network and atypical vascular pattern, in: IEEE International Workshop on Medical Measurement and Applications, IEEE, 2006, pp. 63–67.
[30] W.V. Stoecker, K. Gupta, R.J. Stanley, R.H. Moss, B. Shrestha, Detection of asymmetric blotches in dermoscopy images of malignant melanoma using relative color, Skin Res. Technol. 11 (2005) 179–184.
[31] A. Khan, K. Gupta, R.J. Stanley, W.V. Stoecker, R.H. Moss, G. Argenziano, H.P. Soyer, H.S. Rabinovitz, A.B. Cognetta, Fuzzy logic techniques for blotch feature evaluation in dermoscopy images, Comput. Med. Imaging Graph. 33 (2009) 50–57.
[32] V.K. Madasu, B.C. Lovell, Blotch detection in pigmented skin lesions using fuzzy co-clustering and texture segmentation, in: 2009 Digital Image Computing: Techniques and Applications, IEEE, 2009, pp. 25–31.
[33] A. Dalal, R.H. Moss, R.J. Stanley, W.V. Stoecker, K. Gupta, D.A. Calcara, J. Xu, B. Shrestha, R. Drugge, J.M. Malters, L.A. Perry, Concentric decile segmentation of white and hypopigmented areas in dermoscopy images of skin lesions allows discrimination of malignant melanoma, Comput. Med. Imaging Graph. 35 (2011) 148–154.
[34] W.V. Stoecker, M. Wronkiewiecz, R. Chowdhury, R.J. Stanley, J. Xu, A. Bangert, B. Shrestha, D.A. Calcara, H.S. Rabinovitz, M. Oliviero, F. Ahmed, L.A. Perry, R. Drugge, Detection of granularity in dermoscopy images of malignant melanoma using color and texture features, Comput. Med. Imaging Graph. 35 (2011) 144–147.
[35] H. Iyatomi, H. Oka, M.E. Celebi, K. Ogawa, G. Argenziano, H.P. Soyer, H. Koga, T. Saida, K. Ohara, M. Tanaka, Computer-based classification of dermoscopy images of melanocytic lesions on acral volar skin, J. Investig. Dermatol. 128 (2008) 2049–2054.
[36] M.G. Fleming, C. Steger, J. Zhang, J. Gao, A.B. Cognetta, L. Pollak, C.R. Dyer, Techniques for a structural analysis of dermatoscopic imagery, Comput. Med. Imaging Graph. 22 (1998) 375–389.
[37] M. Anantha, R.H. Moss, W.V. Stoecker, Detection of pigment network in dermatoscopy images using texture analysis, Comput. Med. Imaging Graph. 28 (2004) 225–234.
[38] T. Lee, V. Ng, R. Gallagher, A. Coldman, D. McLean, Dullrazor: a software approach to hair removal from images, Comput. Biol. Med. 27 (1997) 533–543.
[39] C. Grana, R. Cucchiara, G. Pellacani, S. Seidenari, Line detection and texture characterization of network patterns, in: 18th International Conference on Pattern Recognition (ICPR'06), vol. 2, IEEE, 2006, pp. 275–278.

[40] G. Di Leo, C. Liguori, A. Paolillo, P. Sommella, An improved procedure for the automatic detection of dermoscopic structures in digital ELM images of skin lesions, in: 2008 IEEE Conference on Virtual Environments, Human-Computer Interfaces and Measurement Systems, IEEE, 2008, pp. 190–194.
[41] B. Shrestha, J. Bishop, K. Kam, X. Chen, R.H. Moss, W.V. Stoecker, S. Umbaugh, R.J. Stanley, M.E. Celebi, A.A. Marghoob, G. Argenziano, H.P. Soyer, Detection of atypical texture features in early malignant melanoma, Skin Res. Technol. 16 (2010) 60–65.
[42] M. Sadeghi, M. Razmara, T.K. Lee, M.S. Atkins, A novel method for detection of pigment network in dermoscopic images using graphs, Comput. Med. Imaging Graph. 35 (2011) 137–143.
[43] M. Sadeghi, M. Razmara, P. Wighton, T.K. Lee, M.S. Atkins, Modeling the dermoscopic structure pigment network using a clinically inspired feature set, in: Lecture Notes in Computer Science, vol. 6326, 2010, pp. 467–474.
[44] S.O. Skrovseth, T.R. Schopf, K. Thon, M. Zortea, M. Geilhufe, K. Mollersen, H.M. Kirchesch, F. Godtliebsen, A computer aided diagnostic system for malignant melanomas, in: 2010 3rd International Symposium on Applied Sciences in Biomedical and Communication Technologies (ISABEL 2010), IEEE, 2010, pp. 1–5.
[45] P. Wighton, T.K. Lee, H. Lui, D.I. McLean, M.S. Atkins, Generalizing common tasks in automated skin lesion diagnosis, IEEE Trans. Inf. Technol. Biomed. 15 (2011) 622–629.
[46] C. Barata, J.S. Marques, J. Rozeira, A system for the detection of pigment network in dermoscopy images using directional filters, IEEE Trans. Bio-med. Eng. 59 (2012) 2744–2754.
[47] L.G. Shapiro, G.C. Stockman, Computer Vision, Prentice Hall, 2001.
[48] T. Gevers, A.W.M. Smeulders, Color-based object recognition, Pattern Recognit. 32 (1999) 453–464.
[49] R.M. Haralick, K. Shanmugam, I. Dinstein, Textural features for image classification, IEEE Trans. Syst. Man Cybern. 3 (1973) 610–621.
[50] A. Baraldi, F. Parmiggiani, An investigation of the textural characteristics associated with gray level cooccurrence matrix statistical parameters, IEEE Trans. Geosci. Remote Sens. 33 (1995) 293–304.
[51] D.A. Clausi, An analysis of co-occurrence texture statistics as a function of grey level quantization, Can. J. Remote Sens. 28 (2002) 45–62.
[52] J.R. Quinlan, C4.5: Programs for Machine Learning, Morgan Kaufmann, San Francisco, CA, 1993.
[53] The University of Waikato, WEKA, 2013, http://www.cs.waikato.ac.nz/ml/weka (Online accessed 10-Oct-2013).
[54] G. Argenziano, H.P. Soyer, V.D.G.D. Piccolo, P. Carli, M. Delfino, A. Ferrari, R. Hofmann-Wellenhof, D. Massi, G. Mazzocchetti, M. Scalvenzi, I.H. Wolf, Interactive Atlas of Dermoscopy, 2001.